link.springer.com link.springer.com

Published online 16 August 2021 | https://doi.org/10.1007/s40843-021-1711-5
Sci China Mater 2021, 64(11): 2846–2857

First- and second-order phase transitions in RE_6Co_2Ga (RE = Ho, Dy or Gd) cryogenic magnetocaloric materials

Dan Guo[1,2], Luis M. Moreno-Ramírez[2], Carlos Romero-Muñiz[3,4], Yikun Zhang[1*], Jia-Yan Law[2*], Victorino Franco[2], Jiang Wang[1] and Zhongming Ren[1]

ABSTRACT **Rare-earth (RE) rich intermetallics crystallizing in orthorhombic Ho_6Co_2Ga-type crystal structure exhibit peculiar magnetic properties that are not widely reported for their magnetic ordering, order of magnetic phase transition, and related magnetocaloric behavior. By tuning the type of RE element in RE_6Co_2Ga (RE = Ho, Dy or Gd) compounds, metamagnetic anti-to-paramagnetic (AF to PM) phase transitions could be tuned to ferro-to-paramagnetic (FM to PM) phase transitions. Furthermore, the FM ground state for Gd_6Co_2Ga is confirmed by density functional theory calculations in addition to experimental observations. The field dependence magnetocaloric and Banerjee's criteria demonstrate that Ho_6Co_2Ga and Dy_6Co_2Ga undergo a first-order phase transition in addition to a second-order phase transition, whereas only the latter is observed for Gd_6Co_2Ga. The two extreme alloys of the series, Ho_6Co_2Ga and Gd_6Co_2Ga, show maximum isothermal entropy change ($|\Delta S_{iso}{}^{max}(5\,T)|$) of 10.1 and 9.1 $J\,kg^{-1}\,K^{-1}$ at 26 and 75 K, close to H_2 and N_2 liquefaction, respectively. This outstanding magnetocaloric effect performance makes the RE_6Co_2Ga series of potential for cryogenic magnetic refrigeration applications.**

Keywords: RE_6Co_2Ga compounds, magnetic phase transitions, magnetocaloric effect, rare-earth

INTRODUCTION

The pursuit of energy conservation and environmental protection has become the mainstream of modern society. The vapor-compression refrigeration, a widely used technology in transportation, and residential, commercial, and industrial refrigeration, can no longer meet the current development needs due to its low efficiency, adverse environmental impact, and noise of the compressor. Several researchers have shifted their focus to magnetic refrigeration (MR) based on the magnetocaloric effect (MCE) of magnetic materials due to their distinguished performance without relying on any hazardous or ozone-depleting refrigerant gas and noise-free advantage [1–7]. The use of natural gas as well as H_2, He, N_2, and O_2, is widely extended with several scientific, industrial, and commercial purposes. Moreover, their consumption is expected to increase in future years. For better gas storage and transport, gas liquefaction is required despite being a complex process [8]. In recent years, it has been shown that MR technology could overcome some of the issues related to conventional methods [9,10]. Therefore, it is of significance to search for MCE materials suitable for cryogenic MR applications. The performance of MCE materials can be evaluated by the magnetic entropy change in an isothermal process (ΔS_{iso}) and/or temperature change in an adiabatic process (ΔT_{ad}), which are correlated to thermomagnetic phase transitions of the materials. In general, MCE materials are classified into the order of thermomagnetic phase transitions they undergo. For those undergoing first-order phase transition (FOPT), they usually exhibit large ΔS_{iso} values, but their accompanying thermal and magnetic hystereses can affect their cyclicality. On the other hand, for those exhibiting

[1] State Key Laboratory of Advanced Special Steels, Shanghai Key Laboratory of Advanced Ferrometallurgy, School of Materials Science and Engineering, Shanghai University, Shanghai 200072, China
[2] Departamento de Física de la Materia Condensada, ICMS-CSIC, Universidad de Sevilla, P.O. Box 1065, Sevilla 41080, Spain
[3] Department of Physical, Chemical and Natural Systems, Universidad Pablo de Olavide, Sevilla E-41013, Spain
[4] Departamento de Física Aplicada I, Universidad de Sevilla, Sevilla E-41012, Spain
* Corresponding authors (emails: ykzhang@shu.edu.cn (Zhang Y); jylaw@us.es (Law JY))

second-order phase transition (SOPT), while they exhibit no hysteresis, their ΔS_{iso} values may be lower than those of FOPT materials [11–13].

In the past decade, a large number of MCE materials have been reported [14–20], among which rare-earth (RE) based alloys show great significance for MR applications at cryogenic temperatures. In particular, those crystallizing in orthorhombic Ho_6Co_2Ga-type structures (space group *Immm*) could exhibit both inverse (positive ΔS_{iso} under magnetization process) and direct MCE (negative ΔS_{iso} under magnetization process) despite showing peculiar and complex magnetic behavior [21–36]. For example, S-shaped curves of magnetization *versus* magnetic field $M(H)$ were reported for $RE_6Co_x(Al/Sn)_y$ (x = 2.2–2.5 and y = 0.5–0.8), whereby all of them adopted the Ho_6Co_2Ga-type structure [21–23]. Inverse and direct MCE were then reported for isostructural $Dy_6Co_{2.5}Sn_{0.5}$ [21] and $RE_6Co_{2.2}Al_{0.8}$ (RE = Dy or Tb) [22], in which authors suggested that the magnetic ordering of Ho_6Co_2Ga-type compounds is determined by the orthorhombically distorted octahedral RE sublattice, which in turn can yield similar magnetic structure and properties for such compounds despite their selection for the elements. Overall, these investigations centered on using compositions that can crystallize into orthorhombic Ho_6Co_2Ga-type structure; nevertheless, the studies on nominal RE_6Co_2Ga compositions, which are directly adopted from the structure itself, are less reported [24,25] and mainly on their crystal structures while their thermomagnetic and MCE properties have not been explored.

Hence, in this paper, we aim to systematically investigate the influence of various RE elements on the structures, thermomagnetic phase transitions, and magnetocaloric properties of RE_6Co_2Ga-type compounds by changing RE from Ho to Dy and Gd. Using the recently developed criterion based on MCE [37] and the conventional Banerjee's criterion [38], we report the nature of the order of magnetic phase transition undergone by these compounds. It is found that the Ho- and Dy-containing compounds exhibit low-temperature FOPT while the Gd-containing one exhibits SOPT. Density functional theory (DFT) calculations are performed for these compounds, further supporting the magnetic ordering observed from the experimental results.

EXPERIMENTAL AND SIMULATION DETAILS

Polycrystalline samples with nominal compositions of RE_6Co_2Ga (RE = Ho, Dy or Gd) were synthesized by arc melting from raw pure materials RE (99.9 %), Co (99.9 %) and Ga (99.999 %) in an argon atmosphere. Since RE elements could be easily volatilized during melting, 2 wt.% excess was added to ensure the nominal stoichiometry. The ingots were re-melted four times for good compositional homogeneity. They were sealed in a quartz tube filled with argon and then annealed in a muffle furnace at 600°C for seven days, followed by quenching with ice water. X-ray diffraction (XRD) patterns of the samples at room temperature were collected by a Bruker D8 diffractometer (Cu-Kα radiation) for studying their microstructures. Magnetization measurements were carried out using the vibrating sample magnetometer (VSM) option of the physical properties measurement system (PPMS-9). ΔS_{iso}, one of the parameters to quantify the MCE of materials, was indirectly determined from the measured magnetic isotherms using thermodynamic Maxwell relation:

$$\Delta S_{iso}(T,H) = \mu_0 \int_0^H \left(\frac{\partial M(T,H)}{\partial T} \right)_H \mathrm{d}H, \quad (1)$$

where M, H, and T represent the magnetization, magnetic field, and temperature, respectively. In order to investigate the order of the phase transition by the novel MCE criterion, the field-dependent exponent of ΔS_{iso}, was calculated from the following formula [37]:

$$n(T,H) = \frac{\mathrm{d}\ln|\Delta S_{iso}|}{\mathrm{d}\ln H}. \quad (2)$$

In addition, DFT calculations were performed for unveiling the magnetic behavior of RE_6Co_2Ga compounds, whereby we exclusively focused on Gd_6Co_2Ga as the latest and the most sophisticated DFT methods are limited in accurately describing the complex magnetic behavior of some RE elements, such as Ho and Dy. For this purpose, we employed the standard Vienna *Ab-initio* Simulation Package (VASP) 5.4.1 [39], using plane waves to reproduce the one-electron wave functions with a kinetic energy cutoff of 400 eV for constructing the basis set and projected augmented wave pseudopotentials [40,41] for all the species involved. In particular, the valence electrons excluded in the pseudopotentials were $3d^84s^1$ (9) in Co, $4s^24p^1$ (3) in Ga and $5s^25p^64f^75d^16s^2$ (18) in Gd. Thus, the f electrons of Gd were explicitly considered to properly describe its magnetism. The electronic exchange and correlation were modeled using a hybrid functional, namely the HSE06, which contained 25% of exact Hartree-Fock as exchange, following the implementation of the VASP code [42,43]. As a start, the standard Perdew-Burke-Ernzerhof (PBE) functional [44] was used but it was later found insufficient for such a complex system. In particular, it failed when resolving the on-site magnetism

of the compound. As spin polarization was required for all calculations, we used the Vosko-Wilk-Nusair interpolation [45] for this task.

Using the geometry provided by XRD data [24] for the analysis of the compound, structural optimizations using a conjugate gradient algorithm, sampling the reciprocal space with a 4 × 4 × 4 Monkhorst-pack grid, were performed until forces upon atoms were smaller than 0.01 eV Å^{-1}, and each self-consistent electronic loop converged to a tolerance better than 10^{-4} eV [46]. At PBE level, the obtained structure remains very similar to the experimental configuration with minimal displacement in atomic coordinates (only up to 0.1 Å in the worse scenario). This relaxed structure was further analyzed using the HSE06 hybrid functional. In all cases, we deal with a primitive 18-atom cell, which corresponds to a Niggli reduced cell. This is a quasi-rhombohedral unit cell (with a = 8.323 Å, α = 107.25°, β = 109.96°, and γ = 111.23°) generated using the VESTA software [47]. It possesses a unit cell volume and a number of atoms that are small enough to allow calculations with hybrid functionals despite the high proportion of RE metals. Even in that case, we had to reduce the k-point grid to a 2 × 2 × 2 mesh due to the enormous computational demand.

RESULTS AND DISCUSSION

Crystal structure

XRD patterns for the RE_6Co_2Ga (RE = Ho, Dy or Gd) series at room temperature and their corresponding Rietveld refinement results are shown in Fig. 1. The results show that all the samples successfully crystallize into a single phase Ho_6Co_2Ga-type structure. Details of the refined lattice parameters and the refinement factors are tabulated in Table 1, which shows that the cell volume and lattice parameters increase as RE changes from Ho to Dy and Gd. The c cell parameter for Dy_6Co_2Ga (9.8153 Å) is smaller than those for $Dy_6Co_{2.5}Sn_{0.5}$ (9.8754 Å) and Dy_6Co_2Al (9.9265 Å), which is in line with Ref. [22] whereby authors predicted that lattice parameter c increases from Ga to Sn and Al in RE_6Co_2X compounds. Fig. 2a and b illustrate the detailed crystal structures of the RE_6Co_2Ga compounds and the atomic environments of RE1, RE2, RE3, Co1, Co2, Ga1, and Ga2 sites. The Wyckoff sites of RE1, RE2, RE3 atoms are 8*l*, 8*m*, and 8*n* with the ..*m*, .*m*., and *m*.. point symmetry, respectively. Co1 and Co2 atoms occupy the Wyckoff sites of 4*i* and 4*h* with the *mm*2 and *m*2*m* point symmetry, respectively. Ga1 occupies the 2*b* sites with the *mmm* point symmetry and Ga2 occupies the 2*d* sites with the *mmm* point symmetry.

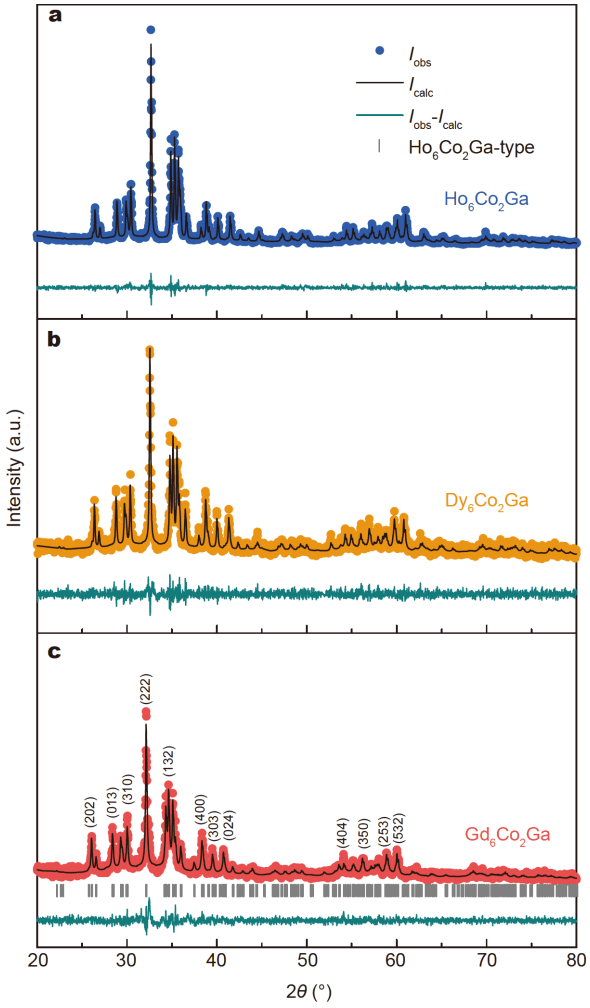

Figure 1 The XRD patterns and their corresponding Rietveld refinements for Ho_6Co_2Ga (a), Dy_6Co_2Ga (b), and Gd_6Co_2Ga (c).

Magnetic properties

Fig. 3 displays the $M(T)$ curves and their reciprocal susceptibility ($1/\chi = H/M$) under a magnetic field of 0.5 T. Ho_6Co_2Ga (Fig. 3a) shows a magnetic phase transition from antiferromagnetic to paramagnetic (AF to PM) at around 16 K and a plateau at 16–25 K, followed by a paramagnetic behavior. For Dy_6Co_2Ga in Fig. 3b, a phase transition from AF to PM is noticed at ~47 K, with the subsequent paramagnetic behavior at higher temperatures. Gd_6Co_2Ga shows three consecutive features at around 55, 78, and 129 K (pointed by the arrows), indicating three thermomagnetic phase transitions (Fig. 3c). The effective magnetic moment values (μ_{eff}) and paramagnetic Curie temperature (θ_P) were deduced by the fittings of the linear part of the $1/\chi$-T plots, yielding:

Table 1 Refined lattice parameters and refinement factors for RE_6Co_2Ga compounds

Parameter	a (Å)	b (Å)	c (Å)	V (Å^3)	α (°)	β (°)	γ (°)	R_p (%)	R_{wp} (%)	R_{exp} (%)	χ^2
Ho_6Co_2Ga	9.2710	9.4078	9.8153	856.09	90	90	90	5.59	7.07	6.03	1.37
Dy_6Co_2Ga	9.2891	9.4654	9.8439	865.53	90	90	90	7.48	9.48	8.79	1.16
Gd_6Co_2Ga	9.3863	9.5968	9.9799	898.97	90	90	90	8.46	10.9	9.75	1.25

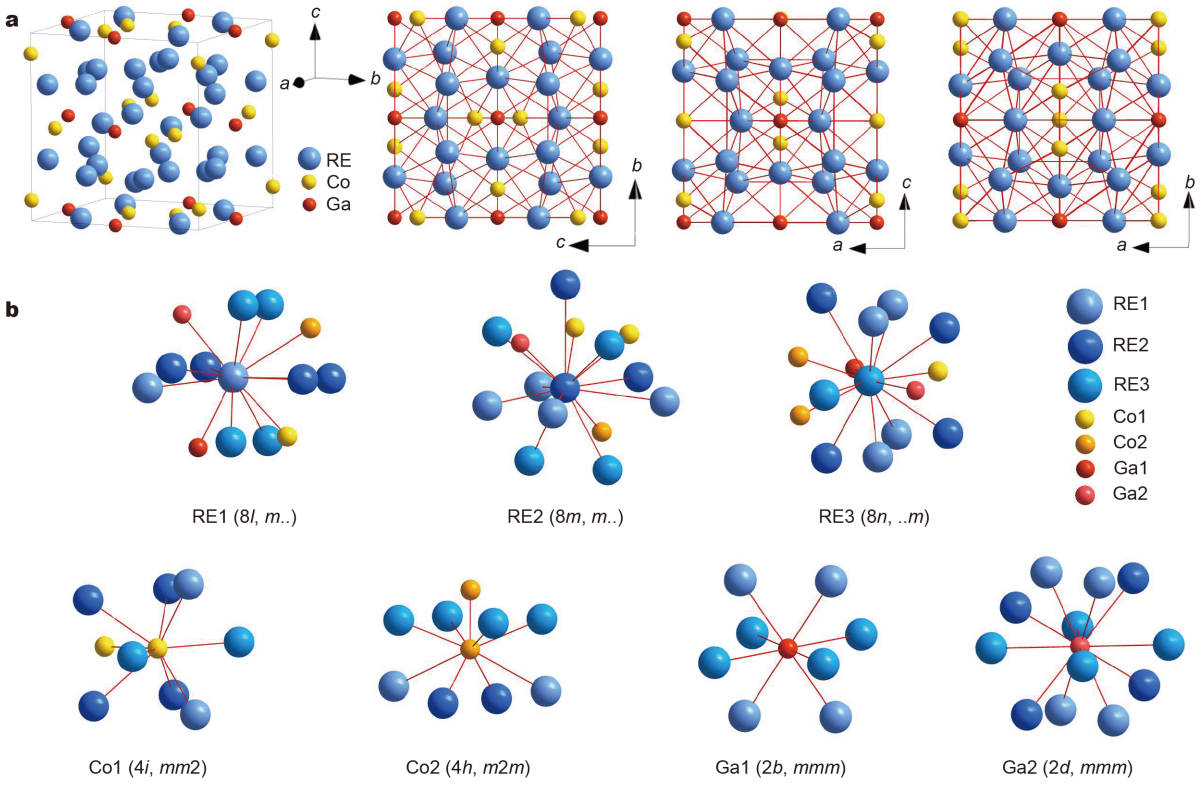

Figure 2 (a) The crystal structures of RE_6Co_2Ga compounds; (b) atomic environments of RE1, RE2, RE3, Co1, Co2, Ga1, and Ga2 sites.

μ_{eff}/f.u. = 29.105 ± 0.006 μ_B, 29.629 ± 0.007 μ_B, and 21.635 ± 0.020 μ_B for Ho_6Co_2Ga, Dy_6Co_2Ga, and Gd_6Co_2Ga, respectively.Assuming the effective magnetic moment of Co atoms is 1.8 μ_B, the effective magnetic moment per RE atom for all three compounds can be calculated from $\mu_{eff} = \sqrt{6 \times \mu_{eff}^2(\mathrm{RE}) + 2 \times \mu_{eff}^2(\mathrm{Co})}$, resulting in μ_{eff}(Ho) = 11.837 ± 0.002 μ_B, μ_{eff}(Dy) = 12.051 ± 0.003 μ_B and μ_{eff}(Gd) = 8.771 ± 0.008 μ_B. The calculated θ_P values are ~1.5, ~3.2, and ~99.1 K for Ho_6Co_2Ga, Dy_6Co_2Ga, and Gd_6Co_2Ga, respectively. In the cases of Ho_6Co_2Ga and Dy_6Co_2Ga, the θ_P values are close to zero, which indicates that there are almost no ferromagnetic (FM) interactions in PM regions.

The zero-field-cooled (ZFC) and field-cooled (FC) $M(T)$ curves for H = 0.05 T of Ho_6Co_2Ga, Dy_6Co_2Ga, and Gd_6Co_2Ga are shown in Fig. S1. A small splitting in FC and ZFC $M(T)$ curves for Gd_6Co_2Ga and Dy_6Co_2Ga is detected at low temperatures, which could probably be due to the domain wall pinning effects [48]. At higher temperatures, the ZFC and FC curves are well overlapped with each other for all the compounds, demonstrating no thermal hysteresis during their magnetic phase transitions. Such absence/negligible thermal hysteresis even in the first-order transformations for RE-based alloys makes these materials highly interesting from a technical point of view [49–51].

Fig. 4 displays the field dependence of magnetization measured at 3 K. Weak magnetic hysteresis can be observed in Ho_6Co_2Ga and Dy_6Co_2Ga, which is common in FOPT materials. For Gd_6Co_2Ga, there is no hysteresis, which is beneficial to practical applications. It can be seen

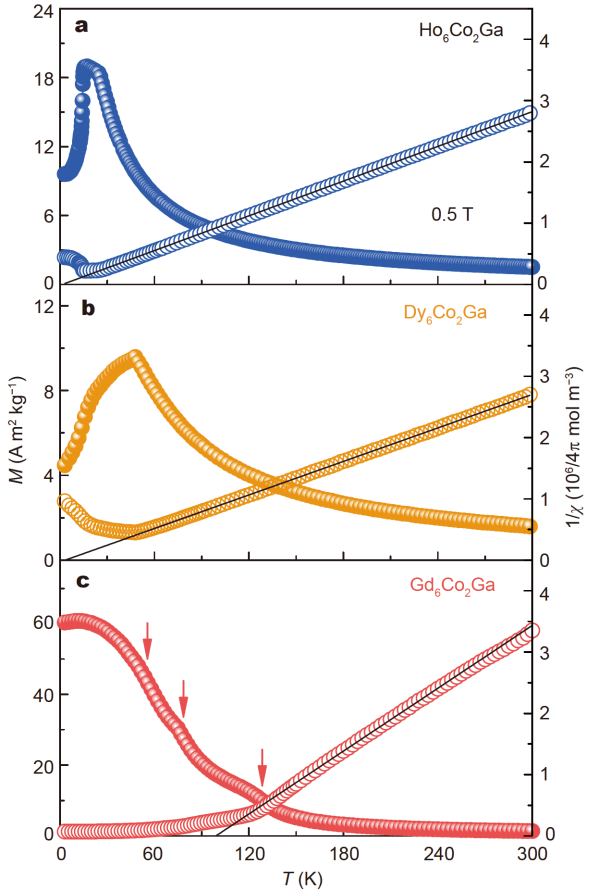

Figure 3 Temperature dependence of magnetization (left-axis) and reciprocal susceptibility (right-axis) under a field of 0.5 T for Ho_6Co_2Ga (a), Dy_6Co_2Ga (b), and Gd_6Co_2Ga (c).

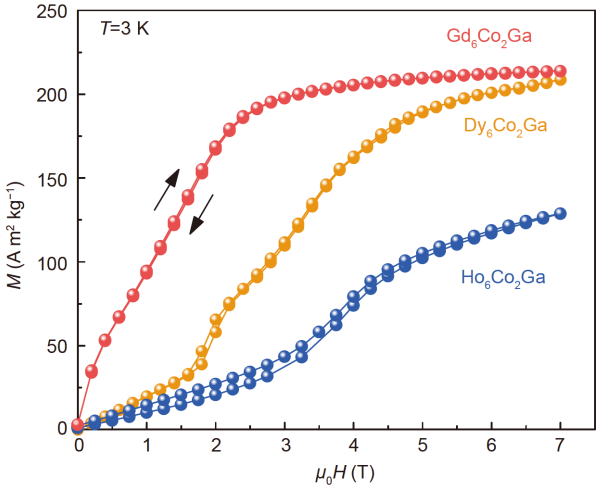

Figure 4 The field dependence of magnetization measured at 3 K.

that the magnetization isotherms for Ho_6Co_2Ga and Dy_6Co_2Ga compounds show a significant increase for certain applied magnetic fields (fields between 2 and 4.5 T for Ho_6Co_2Ga and Dy_6Co_2Ga, respectively), indicating the existence of metamagnetic transitions. This is in agreement with the S-shaped $M(H)$ curves previously reported for isostructural Dy_6Co_2Al and Er_6Co_2Al compounds [23]. On the other hand, for Gd_6Co_2Ga, the $M(H)$ shape indicates the FM character at 3 K.

In addition to experimental observations, DFT calculations enable the determination of the distribution of the magnetic moments in Gd_6Co_2Ga by using hybrid functional (the standard generalized gradient approximation fails to describe this issue). In particular, a reasonable geometry very similar to the experimental result is successfully obtained from the calculations using the PBE functional, which suggests a strong FM ground state, or at least, a configuration with a high total magnetic moment. However, if we try to resolve the on-site magnetism, this simple approximation does not lead to a reasonable value for the magnetic moments of Gd atoms, being too small compared with the experimental observations. In addition, the spin moments associated with the Co atoms get unstable, assuming that they have some magnetic moments that are ferro- or antiferromagnetically coupled to the RE elements in the compound. Conversely, more advance functionals, such as the HSE06, which includes 25% of exact Hartree-Fock exchange, could properly reproduce the magnetic behavior of complex Gd_6Co_2Ga compound. Namely, we confirm that the magnetic ground state of Gd_6Co_2Ga corresponds to a state in which all Gd atoms have a strong magnetic moment of about 7.5 μ_B, pointing in the same direction whereas Co atoms couple in the opposite direction with a magnetic moment of around 1.8 μ_B. No magnetic moment is observed for Ga atoms. Only a minimal difference among Gd atoms belonging to different Wyckoff sites is found: the exact values are 7.49–7.51 μ_B (8*l*), 7.64–7.65 μ_B (8*m*), and 7.47 μ_B (8*n*). The same trend is also observed for Co atoms, whose magnetic moments are within the range of 1.77–1.78 μ_B. We have also calculated the spin-resolved projected density of states of the different species present in the Gd_6Co_2Ga compound as shown in Fig. 5. The strong magnetic moments observed for Gd atoms are reflected in their densities of states as strong localized states, mainly appearing around −4 eV spin up below the Fermi level. These states arise from the Gd f orbitals, resembling the fingerprint of the FM phase of pure Gd [52].

In the cases of Ho and Dy in RE_6Co_2Ga compounds, it is not possible to assume any trivial magnetic moment distribution for the constituent atoms that can be compatible with the experimental magnetic moments of RE

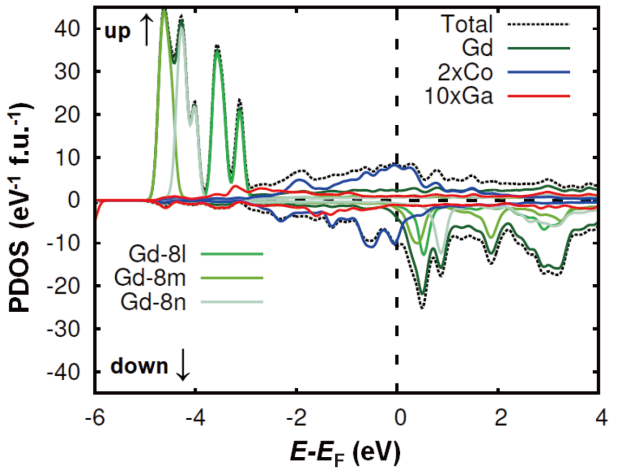

Figure 5 Spin-resolved projected density of states of each species (colored curves) and total density of states (black dotted curve) in Gd_6Co_2Ga calculated with DFT. The contributions of Co (blue) and Ga (red) have been multiplied by a factor to enhance visualization, since their contributions are very small. Contributions arising from the three different Gd sites of the crystal structure (green curves) are plotted together with the total Gd contribution.

atoms. This suggests that the magnetic behavior of these two compounds is much more complex than the case of Gd, which could likely involve non-collinear behavior as reported in other isostructural compounds, such as $Tb_6Co_{2.2}Al_{0.8}$ and Er_6Ni_2Sn [22,36]. The calculated total magnetic moment of Gd_6Co_2Ga lies between 41–45 μ_B per f.u., in good agreement with the experimental saturation magnetization values (43.35 μ_B per f.u. for Gd_6Co_2Ga at 7 T obtained from Fig. 4). It is worth noting that the estimated value is 45 μ_B per f.u., while the summation over the individual contributions of the constituent atoms leads to 41.6 μ_B per f.u. The first estimation is supposed to be a more accurate value for the total magnetic moment.

A large number of possible magnetic configurations as starting guesses for the electronic self-consistency calculation were performed but only two stable configurations were obtained. One is described above, and the second stable configuration is with the total FM solution, which is less energetically favorable. Other explored configurations include possible AFM couplings among Gd atoms belonging to different crystallographic sites, but none of them remain stable. It is interesting to note that the 18-atom primitive cell could still contain an even number for all species in all Wyckoff sites, which is a useful condition needed to properly study possible FM or AFM configurations. We did not find any other stable solution considering AFM couplings among Gd atoms. A similar analysis was also made at PBE level, without finding any reasonable conclusion.

Overall, the results of DFT calculations are in good agreement with the experimental observations of Gd_6Co_2Ga. DFT reveals that the compound exhibits a relatively simple magnetic moment distribution (i.e., parallel Gd atoms with the FM ground state), which agrees with the significant and positive θ_p value (~99.1 K) of Gd_6Co_2Ga. Furthermore, the effective magnetic moment of Gd atoms determined by DFT and experimental results is in reasonable agreement with the theoretical value (7.94 μ_B).

MCE and the order of phase transitions

Fig. 6a–c show the isothermal $M(H)$ curves used for calculating ΔS_{iso} (shown in Fig. 6d–f) for the three studied compounds. Ho_6Co_2Ga and Dy_6Co_2Ga show inverse MCE at low temperatures while their direct MCE are at higher temperatures. In the case of Gd_6Co_2Ga compound, three direct MCE peaks (57, 75, and 131 K) are found in its $\Delta S_{iso}(T)$ curves (being more visible for low magnetic field changes as shown in the inset of Fig. 6f), which correspond to the three phase transitions previously observed in Fig. 3. The most prominent magnetocaloric peak is the one at 75 K. These observations are in agreement with the MCE reports of isostructural compounds, where inverse and direct MCE are found for $Dy_6Co_{2.2}Al_{0.8}$ and $Dy_6Co_{2.5}Sn_{0.5}$ and three observed transitions are in $Gd_6Co_{2.2}Al_{0.8}$ [21,22]. It is worth noting that for low temperatures there is a change of sign for ΔS_{iso}. More detailed studies are needed to identify the origin of that feature. The maximum values of $|\Delta S_{iso}|$ under ΔH of 0–7 T are 15.8, 4.8, and 12.6 $J\,kg^{-1}\,K^{-1}$ for Ho_6Co_2Ga, Dy_6Co_2Ga, and Gd_6Co_2Ga, respectively. It is worth highlighting that the peak temperatures of $|\Delta S_{iso}|$ for the Ho_6Co_2Ga and Gd_6Co_2Ga compounds, 26 and 75 K, respectively, coincide with the desired range for H_2 and N_2 liquefaction. To check the effect of the demagnetizing field on ΔS_{iso}, we considered a demagnetizing factor (N) of 1/3 due to the shape of our samples. The maximum values of isothermal entropy change (ΔS_{iso}^{max}) as a function of the applied field (H_{ap}) and the internal field ($H_{int} = H_{ap} - NM$) for all the compounds are plotted in Fig. S2. Very minor difference can be observed when considering the applied or the internal magnetic field, indicating that the effect of the demagnetizing field can be neglected for the studied samples.

The temperature-averaged magnetic entropy change (TEC), an appropriate parameter to evaluate the MCE materials, has been introduced by Griffith *et al.* [53] and can be calculated by the following equation:

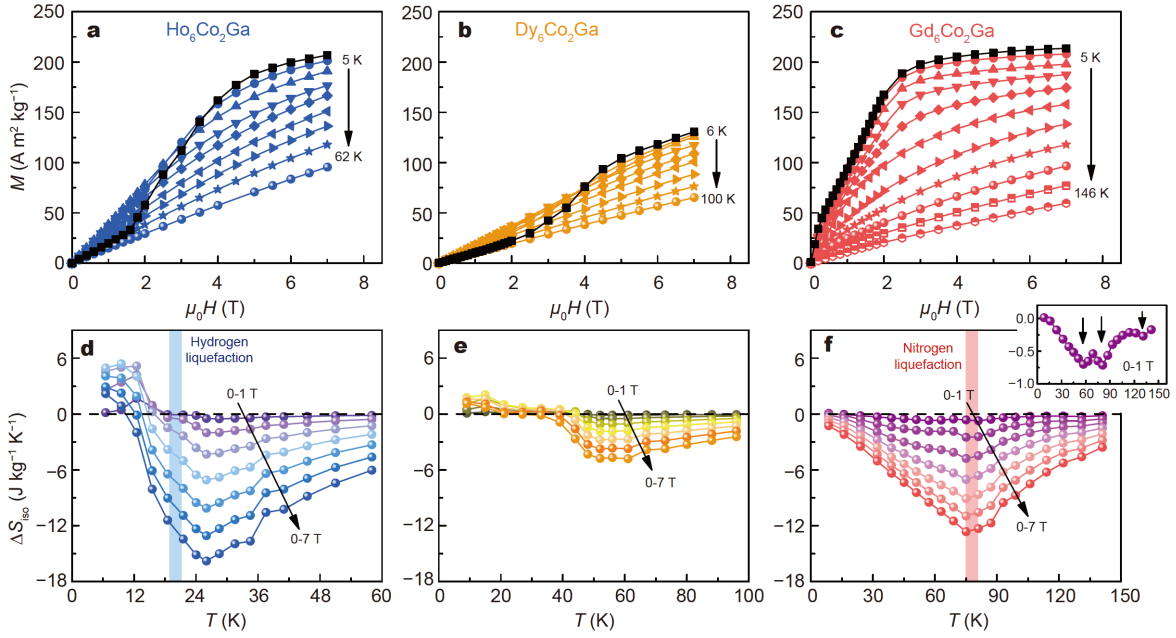

Figure 6 The isothermal magnetization curves at selected temperatures for Ho_6Co_2Ga (a), Dy_6Co_2Ga (b), and Gd_6Co_2Ga (c). The isothermal magnetic entropy changes (ΔS_{iso}) for Ho_6Co_2Ga (d), Dy_6Co_2Ga (e), and Gd_6Co_2Ga (f). The inset of (f) shows the ΔS_{iso}-T curve in the range of 0–1 T for Gd_6Co_2Ga.

$$\mathrm{TEC}(\Delta T_{\mathrm{lift}}) = \frac{1}{\Delta T_{\mathrm{lift}}} \max_{T_{\mathrm{mid}}}\left\{\int_{T_{\mathrm{mid}}-\frac{\Delta T_{\mathrm{lift}}}{2}}^{T_{\mathrm{mid}}+\frac{\Delta T_{\mathrm{lift}}}{2}} \Delta S(T)_{\Delta H,T}\,\mathrm{d}T\right\}, \quad (3)$$

where ΔT_{lift} is temperature span and T_{mid} is the central temperature whereby the TEC (ΔT_{lift}) gets the maximum value for the given ΔT_{lift}. The values of TEC (10) (ΔT_{lift} = 10 K) under field change of 0–7 T are 14.9 J kg^{-1} K^{-1} for Ho_6Co_2Ga, 4.7 J kg^{-1} K^{-1} for Dy_6Co_2Ga and 12.5 J kg^{-1} K^{-1} for Gd_6Co_2Ga, which are close to those of $|\Delta S_{\mathrm{iso}}{}^{\mathrm{max}}|$.

Another magnetocaloric parameter for a figure of merit is the relative cooling power (RCP), which is used to evaluate the cooling efficiency of MCE materials. It can be calculated by the following formula:

$$\mathrm{RCP} = -\Delta S_{\mathrm{iso}}^{\mathrm{max}} \times \delta T_{\mathrm{FWHM}}, \quad (4)$$

where δT_{FWHM} is the full width at half maximum of $|\Delta S_{\mathrm{iso}}|$. The calculated values of RCP under ΔH of 0–7 T are 532.6 J kg^{-1} for Ho_6Co_2Ga, 256.9 J kg^{-1} for Dy_6Co_2Ga, and 945.3 J kg^{-1} for Gd_6Co_2Ga. Due to the three continuous phase transitions in Gd_6Co_2Ga, its refrigerant capacity is significantly higher than those of RE-based compounds reported in the literature. For comparison, the values of $|\Delta S_{\mathrm{iso}}{}^{\mathrm{max}}|$ and RCP of the studied RE_6Co_2Ga (RE = Ho, Dy or Gd) series *versus* those of other isostructural and promising RE-based magnetocaloric materials under a field change of 0–5 T are listed in Table 2 [14,21,22,54–62]. The MCE parameters for the present compounds (especially for Ho_6Co_2Ga and Gd_6Co_2Ga) studied in this work are competitive and even better than those of other reported materials, indicating their potential for cryogenic MR applications. In addition, the Ho_6Co_2Ga and Gd_6Co_2Ga compounds possess similar magnitudes of the isothermal entropy change within a temperature span of 50 K. It has been raised that magnetocaloric composite material systems with the T_C of phases in close proximity can aid performance optimization [63–66]. Therefore, it is worth exploring the MCE properties of a hypothetical composite of these two compounds. Assuming no interactions among the phases, the total values of ΔS_{iso} for $x Ho_6Co_2Ga + (1-x)Gd_6Co_2Ga$ composite (x is the mass fraction of Ho_6Co_2Ga with $0 \le x \le 1$) for ΔH of 0–5 T were estimated as shown in Fig. 7. The optimal table-like MCE is found for x = 0.2, obtaining an RCP of 640 J kg^{-1}, which is larger than those of Ho_6Co_2Ga and Gd_6Co_2Ga. In addition, the maximum temperature span has been found for x = 0.4, improving δT_{FWHM} up to 90 K, which is much larger than that of single Ho_6Co_2Ga and Gd_6Co_2Ga (29 and 68 K, respectively). Such a wide working temperature range (covering the H_2 and N_2 liquefaction temperature ranges) makes it

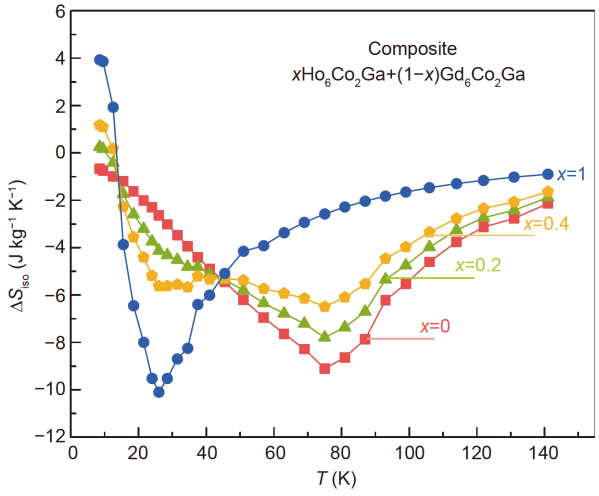

Figure 7 Temperature dependence of ΔS_{iso} for the hypothetical $x$$Ho_6Co_2Ga$ + (1−x)Gd_6Co_2Ga composite for ΔH of 0–5 T.

suitable for cryogenic refrigeration applications. In addition, these estimated phase fractions showing MCE optimization are in agreement with the reports of Ref. [67] in which the larger phase proportion of the higher T_C phase will lead to RCP enhancement.

Fig. 8a and b display the temperature dependence of ΔS_{iso} (under ΔH of 0–1.5 and 0–2.0 T) and exponent n (under ΔH of 0–1.75 T) for the Ho_6Co_2Ga. It has been reported that the overshoot of n above 2 near the transition temperature should be observed in the $n(T)$ curves for FOPT materials [12]. For Ho_6Co_2Ga, it can be observed that n shows large values at low temperatures and in the region that MCE switches from inverse to direct (marked by the cyan box). For the former, the typical whole overshoot is not observed (due to the low transition temperature of Ho_6Co_2Ga), but still, n shows an increase above 2 within the inverse MCE region (below the transition temperature at 0 field), indicating the first-order character of the AF-PM transition [68]. On the other hand, in the shadowed region, the large n values are due to the change of ΔS_{iso} signs, unrelated to the order of phase transitions. In addition, the observed features marked by the gray box are related to the plateau observed in Fig. 3. The temperature dependence of ΔS_{iso} and n for Dy_6Co_2Ga under the same field change as Ho_6Co_2Ga are shown in Fig. 8c and d. The overshoot feature (n above 2) can also be clearly observed at low temperatures, which indicates the FOPT nature. Fig. 8e and f show the temperature dependence of ΔS_{iso} (under ΔH of 0–3.0 and 0–4.0 T) and exponent n (under ΔH of 0–3.5 T) for Gd_6Co_2Ga. The $n(T)$ curve shows three minima, which correspond to the three phase transitions aforementioned in the $M(T)$ results (Fig. 3c). Gd_6Co_2Ga does not show any overshoot of $n > 2$ near the transition temperatures (except the shadowed region where MCE switches signs),

Table 2 The phase transition temperatures T_t as well as the MCE parameters $|\Delta S_{iso}^{max}|$ and RCP for RE_6Co_2Ga compounds compared with some other magnetocaloric materials for cryogenic applications under ΔH = 0–5 T

Material	T_t (K)	$\lvert\Delta S_{iso}^{max}\rvert$ (J kg^{-1} K^{-1})		RCP (J kg^{-1})	Refs.
		Direct MCE	Inverse MCE		
Ho_6Co_2Ga	16	10.1	4.1	292	Present work
Dy_6Co_2Ga	47	2.8	1.6	131	Present work
Gd_6Co_2Ga	55/78/129	9.1	–	618	Present work
$Dy_6Co_{2.2}Al_{0.8}$	30	2.8	3.9	~170	[22]
$Gd_6Co_{2.2}Al_{0.8}$	26/59/80	10.9	–	~760	[22]
$Dy_6Co_{2.5}Sn_{0.5}$	42	2.3	6.5	–	[21]
$Gd_{11}Ni_4In_9$	41/92/135	2.8	~1.0	171	[14]
$DyNiSi_2$	25	4.4	3.6	~70	[54]
$GdCo_2B_2C$	17	10.3	–	238	[55]
Ho_2CoGa_3	10	13.8	–	~383	[56]
Tm_2Co_2Ga	12	11.3	–	152	[57]
EuAgCd	27	13.5	-	321	[58]
$HoCo_{0.3}Ni_{1.7}$	27	18.6	–	~628	[59]
$GdZn_2$	85	8.8	–	530	[60]
GdPdIn	90	4.64	–	464	[61]
$GdNi_2$	70	10.8	–	~518	[62]

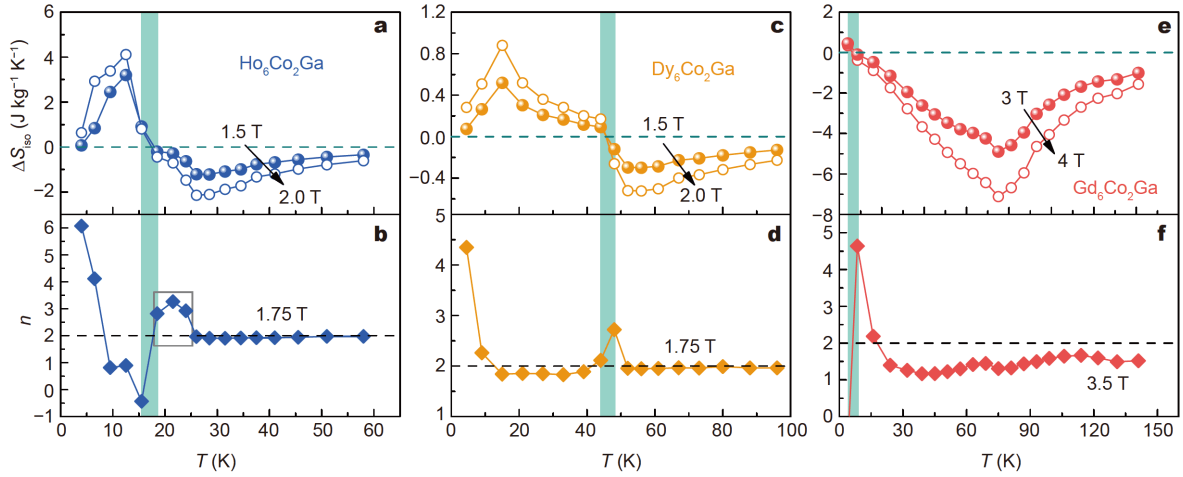

Figure 8 The temperature dependence of ΔS_{iso} and exponent n under different fields for Ho_6Co_2Ga (a, b), Dy_6Co_2Ga (c, d), Gd_6Co_2Ga (e, f).

indicating that the nature of the phase transitions is of second-order. Near the peaks of ΔS_{iso}, n does not show deep minima values below 1 as typically observed at the transition temperatures of single magnetic phase materials, which can be attributed to the mixed phase transitions present in the sample [12].

In addition, the field dependence of ΔS_{iso} and the exponent n were also investigated, as shown in Fig. S3. For Ho_6Co_2Ga and Dy_6Co_2Ga, we chose two temperatures below the inverse MCE peak: 9.5 and 9.0 K, respectively. An obvious overshoot of n above 2 can be found for Ho_6Co_2Ga, evidencing that an AF-PM first-order metamagnetic phase transition occurred [68]. After the phase transition, n decreases down to negative values due to the influence of the direct MCE associated with the FM phase [68]. It is worth noting that an overshoot (slightly above 2) can also be observed for Dy_6Co_2Ga at field changes around 3–4 T, also indicating the first-order character of the AF-PM transition. In the case of Gd_6Co_2Ga, two temperatures after the first two main ΔS_{iso} peaks were chosen: 63 and 87 K. For both temperatures, the values of n are between 1 and 2 due to the coexistence of FM and PM phases. As the transformation begins (see the curve for 63 K), n increases up to 2 followed by decreasing down to values close to 1, indicating the major FM contribution. No overshoot is observed for either temperature, reconfirming the second-order nature of both transitions.

To further evaluate the nature of phase transition, we also studied the Arrott-plots (M^2-H/M) for the three compounds, which are displayed in Fig. 9a–c. Negative slopes are observed for Ho_6Co_2Ga and Dy_6Co_2Ga (being more evident for the former), indicating FOPTs according to Banerjee's criterion [38], which is in agreement with the exponent n criterion. Whereas for Gd_6Co_2Ga, no negative slope or inflection point is observed, demonstrating the second-order nature of the phase transitions. It should be highlighted that there is good agreement between the analyses based on the exponent n criterion and the conventional Banerjee's criterion for this particular series of compounds.

CONCLUSIONS

The structural, magnetic, thermomagnetic, and magnetocaloric properties of RE_6Co_2Ga (RE = Ho, Dy or Gd) compounds were investigated. Rietveld refinement proved the compounds crystallize in single phase Ho_6Co_2Ga-type crystal structure (*Immm* space group). They exhibit complex and interesting magnetic behavior similar to literature work of isostructural $RE_6Co_xA_y$ compounds (A = Al/Sn, x = 2.2–2.5, and y =0.5–0.8). Using the conventional Banerjee's criterion, novel MCE field dependence n fingerprint and DFT studies, the nature of the order of phase transitions, type of phase transitions, and magnetic ordering of such compounds are revealed. Ho_6Co_2Ga and Dy_6Co_2Ga are found to undergo a field-induced first-order AF to PM transition. Gd_6Co_2Ga exhibits FM to PM transition, with three consecutive features found to be of the second-order type. Its DFT calculations unveil its strong FM ground state in agreement with the obtained positive θ_P value and the observed saturated magnetization. By tuning Ho → Gd in RE_6Co_2Ga compounds, FOPT can be obtained in addition to the second-order FM-PM phase transitions: 1st and

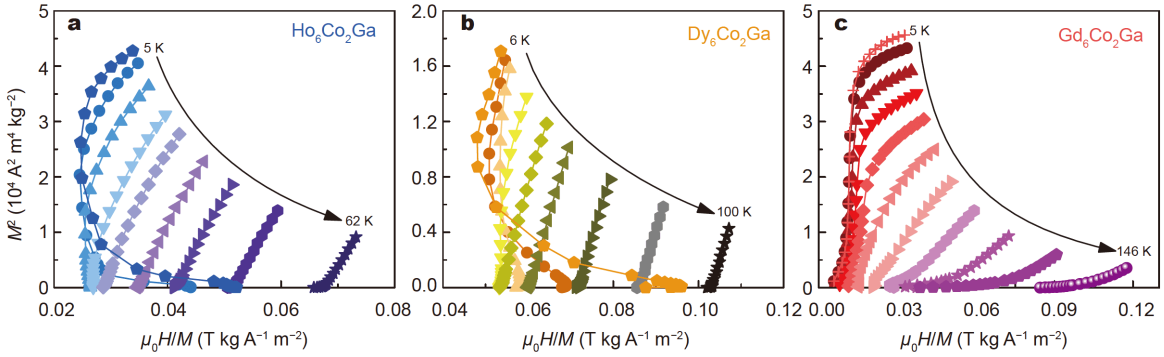

Figure 9 The M^2-H/M curves for Ho_6Co_2Ga (a), Dy_6Co_2Ga (b), and Gd_6Co_2Ga (c).

2nd order for Ho and Dy, and only 2nd order for Gd. This leads to the compounds exhibiting significant MCE performance tunable from 26 to 75 K which falls in the range of H_2 and N_2 liquefaction, indicating their potential applications in cryogenic MR.

Received 16 April 2021; accepted 20 May 2021; published online 16 August 2021

1 Franco V, Blázquez JS, Ipus JJ, *et al.* Magnetocaloric effect: From materials research to refrigeration devices. Prog Mater Sci, 2018, 93: 112–232
2 Li L, Yan M. Recent progresses in exploring the rare earth based intermetallic compounds for cryogenic magnetic refrigeration. J Alloys Compd, 2020, 823: 153810
3 Shen BG, Sun JR, Hu FX, *et al.* Recent progress in exploring magnetocaloric materials. Adv Mater, 2009, 21: 4545–4564
4 Kitanovski A. Energy applications of magnetocaloric materials. Adv Energy Mater, 2020, 10: 1903741
5 Li L, Xu P, Ye S, *et al.* Magnetic properties and excellent cryogenic magnetocaloric performances in B-site ordered RE_2ZnMnO_6 (RE = Gd, Dy and Ho) perovskites. Acta Mater, 2020, 194: 354–365
6 Zhang Y. Review of the structural, magnetic and magnetocaloric properties in ternary rare earth RE_2T_2X type intermetallic compounds. J Alloys Compd, 2019, 787: 1173–1186
7 Law JY, Díaz-García Á, Moreno-Ramírez LM, *et al.* Increased magnetocaloric response of FeMnNiGeSi high-entropy alloys. Acta Mater, 2021, 212: 116931
8 Venkatarathnam G. Cooling and Liquefaction of Air and Its Constituents. New York: Springer, 2008
9 Teyber R, Holladay J, Meinhardt K, *et al.* Performance investigation of a high-field active magnetic regenerator. Appl Energy, 2019, 236: 426–436
10 Zhang H, Gimaev R, Kovalev B, *et al.* Review on the materials and devices for magnetic refrigeration in the temperature range of nitrogen and hydrogen liquefaction. Phys B-Condens Matter, 2019, 558: 65–73
11 Gutfleisch O, Gottschall T, Fries M, *et al.* Mastering hysteresis in magnetocaloric materials. Philos T R Soc A, 2016, 374: 2074
12 Law JY, Franco V, Moreno-Ramírez LM, *et al.* A quantitative criterion for determining the order of magnetic phase transitions using the magnetocaloric effect. Nat Commun, 2018, 9: 2680
13 Moreno-Ramírez LM, Romero-Muñiz C, Law JY, *et al.* Tunable first order transition in $La(Fe,Cr,Si)_{13}$ compounds: Retaining magnetocaloric response despite a magnetic moment reduction. Acta Mater, 2019, 175: 406–414
14 Zhang Z, Wang P, Jia Y, *et al.* Crystal structure, magnetic phase transitions and magnetocaloric effect (MCE) in layer-like $RE_{11}Ni_4In_9$ (RE = Gd, Dy and Ho) compounds. J Alloys Compd, 2021, 851: 155863
15 Yang SX, Zheng XQ, Yang WY, *et al.* Tunable magnetic properties and magnetocaloric effect of TmGa by Ho substitution. Phys Rev B, 2020, 102: 174441
16 Li L, Yuan Y, Qi Y, *et al.* Achievement of a table-like magnetocaloric effect in the dual-phase $ErZn_2$/ErZn composite. Mater Res Lett, 2018, 6: 67–71
17 Zhang Y, Wu B, Guo D, *et al.* Magnetic properties and promising cryogenic magneto-caloric performances of $Gd_{20}Ho_{20}Tm_{20}Cu_{20}Ni_{20}$ amorphous ribbons. Chin Phys B, 2021, 30: 017501
18 Wu B, Zhang Y, Guo D, *et al.* Structure, magnetic properties and cryogenic magneto-caloric effect (MCE) in RE_2FeAlO_6 (RE = Gd, Dy, Ho) oxides. Ceramics Int, 2021, 47: 6290–6297
19 Guo D, Zhang Y, Wang Y, *et al.* Table-like shape magnetocaloric effect and large refrigerant capacity in dual-phase HoNi/$HoNi_2$ composite. Chin Phys B, 2020, 29: 107502
20 Ma Z, Dong X, Zhang Z, *et al.* Achievement of promising cryogenic magnetocaloric performances in $La_{1-x}Pr_xFe_{12}B_6$ compounds. J Mater Sci Tech, 2021, 92: 138–142
21 Morozkin AV, Nirmala R, Malik SK. Magnetic and magnetocaloric properties of Ho_6Co_2Ga-type $Dy_6Co_{2.5}Sn_{0.5}$ compound. J Magn Magn Mater, 2015, 378: 174–177
22 Morozkin AV, Garshev AV, Yapaskurt VO, *et al.* Magnetic ordering of Ho_6Co_2Ga-type {Gd, Tb, Dy}$_6Co_{2.2}Al_{0.8}$ and Tb_6Co_2Al compounds by magnetization and neutron diffraction study. Intermetallics, 2019, 113: 106588
23 Stegemann F, Janka O. Two series of rare earth metal-rich ternary aluminium transition metallides—RE_6Co_2Al (RE = Sc, Y, Nd, Sm, Gd–Tm, Lu) and $RE_6Ni_{2.25}Al_{0.75}$ (RE = Y, Gd–Tm, Lu). Z für Naturforsch B, 2018, 73: 927–942
24 Sichevich OM, Komarovskaya LP, Gun YN, *et al.* Crystal structure and magnetic properties of $R_6Ga(Co, Ni)_2$ and R_6SnNi_2 compounds (R is a rare-earth metal). Ukr Fiz Zh, 1984, 29: 1342–1345
25 Gladyshevskii RE, Grin YN, Yarmolyuk YP. Crystal structure of R_6GaCo_2 compounds (R = Y, Dy, Tb, Ho, Er, Tm, Lu), Dopov. Akad Nauk Ukr RSR Ser A, 1983, 2: 67–70

26 Demchyna M, Belan B, Manyako M, *et al.* Phase equilibria in the Dy-Fe-In system and crystal structure of $Dy_6Fe_{1.72}In$. Intermetallics, 2013, 37: 22–26
27 Verbovytskyy Y, Łątka K, Przewoźnik J, *et al.* Crystal structure and magnetic properties of the selected phases from the R-{Co, Ni}-Al (R = Y, Gd-Tm) systems. J Alloys Compd, 2018, 758: 122–130
28 Morozkin AV, Garshev AV, Knotko AV, *et al.* The Gd-Co-Al system at 870/1070 K as a representative of the rare earth-Co-Al family and new rare-earth cobalt aluminides: Crystal structure and magnetic properties. J Solid State Chem, 2018, 261: 62–74
29 Kalychak JM, Zaremba VI, Zavalij PY. Crystal structure of holmium cobalt indium (6/2/1), $Ho_6Co_{2+x}In_{1-x}$, x = 0.135. Z für Kristallogr Crystline Mater, 1993, 208: 380–381
30 Kalychak YM. Composition and crystal structure of rare-earths-Co-In compounds. J Alloys Compd, 1999, 291: 80–88
31 Chen JW, Jou NS, Wang BK, *et al.* Superconductivity and magnetism of the R_6Ni_2Sn (R = Y and rare earth) compounds. Phys B-Condens Matter, 2005, 359-361: 211–213
32 Tyvanchuk YB, Lukachuk M, Pöttgen R, *et al.* The ternary system Tm-Ni-In at 870 K. Z für Naturforsch B, 2015, 70: 665–670
33 Morozkin AV, Garshev AV, Knotko AV, *et al.* The Tb-Co-Ga system at 870 K as a representative of rare-earth cobalt gallides: Crystal structure and magnetic properties. J Solid State Chem, 2019, 277: 303–315
34 Gulay LD, Wołcyrz M. Crystal structure of $R_6Co_{2+x}Pb_{1-y}$ (R = Y, Gd, Tb, Dy, Ho, Er, Tm, Lu) and $R_6Ni_{2+x}Pb_{1-y}$ (R = Tb, Dy, Ho, Er, Tm, Lu) compounds. J Alloys Compd, 2001, 315: 164–168
35 Zaremba RI, Kalychak YM, Rodewald UC, *et al.* New indides $Sc_6Co_{2.18}In_{0.82}$, $Sc_{10}Ni_9In_{19.44}$ and $ScCu_4In$—synthesis, structure, and crystal chemistry. Z für Naturforsch B, 2006, 61: 942–948
36 Prokeš K, Sechovský V, Syshchenko O. Magnetic structure of Er_6Ni_2Sn. J Alloys Compd, 2009, 467: 48–53
37 Franco V, Conde A. Scaling laws for the magnetocaloric effect in second order phase transitions: From physics to applications for the characterization of materials. Int J Refrig, 2010, 33: 465–473
38 Banerjee BK. On a generalised approach to first and second order magnetic transitions. Phys Lett, 1964, 12: 16–17
39 Kresse G, Furthmüller J. Efficient iterative schemes for *ab initio* total-energy calculations using a plane-wave basis set. Phys Rev B, 1996, 54: 11169–11186
40 Blöchl PE. Projector augmented-wave method. Phys Rev B, 1994, 50: 17953–17979
41 Kresse G, Joubert D. From ultrasoft pseudopotentials to the projector augmented-wave method. Phys Rev B, 1999, 59: 1758–1775
42 Heyd J, Scuseria GE, Ernzerhof M. Hybrid functionals based on a screened Coulomb potential. J Chem Phys, 2003, 118: 8207–8215
43 Krukau AV, Vydrov OA, Izmaylov AF, *et al.* Influence of the exchange screening parameter on the performance of screened hybrid functionals. J Chem Phys, 2006, 125: 224106
44 Perdew JP, Burke K, Ernzerhof M. Generalized gradient approximation made simple. Phys Rev Lett, 1996, 77: 3865–3868
45 Vosko SH, Wilk L, Nusair M. Accurate spin-dependent electron liquid correlation energies for local spin density calculations: A critical analysis. Can J Phys, 1980, 58: 1200–1211
46 Monkhorst HJ, Pack JD. Special points for Brillouin-zone integrations. Phys Rev B, 1976, 13: 5188–5192
47 Momma K, Izumi F. VESTA 3 for three-dimensional visualization of crystal, volumetric and morphology data. J Appl Crystlogr, 2011, 44: 1272–1276
48 Zhang XX, Hernàndez JM, Tejada J, *et al.* Magnetic properties and domain-wall motion in single-crystal $BaFe_{10.2}Sn_{0.74}Co_{0.66}O_{19}$. Phys Rev B, 1996, 53: 3336–3340
49 Alho BP, Ribeiro PO, von Ranke PJ, *et al.* Free-energy analysis of the nonhysteretic first-order phase transition of Eu_2In. Phys Rev B, 2020, 102: 134425
50 Biswas A, Zarkevich NA, Pathak AK, *et al.* First-order magnetic phase transition in Pr_2In with negligible thermomagnetic hysteresis. Phys Rev B, 2020, 101: 224402
51 Guillou F, Pathak AK, Paudyal D, *et al.* Non-hysteretic first-order phase transition with large latent heat and giant low-field magnetocaloric effect. Nat Commun, 2018, 9: 2925
52 Oroszlány L, Deák A, Simon E, *et al.* Magnetism of gadolinium: A first-principles perspective. Phys Rev Lett, 2015, 115: 096402
53 Griffith LD, Mudryk Y, Slaughter J, *et al.* Material-based figure of merit for caloric materials. J Appl Phys, 2018, 123: 034902
54 Zhang B, Zheng XQ, Zhang Y, *et al.* Magnetic properties and magnetocaloric effects of $RNiSi_2$ (R = Gd, Dy, Ho, Er, Tm) compounds. AIP Adv, 2018, 8: 056423
55 Zhang Y, Guo D, Wu B, *et al.* Magnetic properties and magnetocaloric performances in $RECo_2B_2C$ (RE = Gd, Tb and Dy) compounds. J Alloys Compd, 2020, 817: 152780
56 Wang LC, Cui L, Dong QY, *et al.* Large magnetocaloric effect with a wide working temperature span in the R_2CoGa_3 (R = Gd, Dy, and Ho) compounds. J Appl Phys, 2014, 115: 233913
57 Zhang Y, Guo D, Geng S, *et al.* Structure, magnetic and cryogenic magneto-caloric properties in intermetallic gallium compounds RE_2Co_2Ga (RE = Dy, Ho, Er, and Tm). J Appl Phys, 2018, 124: 043903
58 Klenner S, Zhang Z, Pöttgen R, *et al.* Magnetic and magnetocaloric properties of the equiatomic europium intermetallics EuAgZn, EuAgCd, EuPtZn and EuAuCd. Intermetallics, 2020, 120: 106765
59 Lai J, Tang X, Sepehri-Amin H, *et al.* Tuning magnetocaloric effect of $Ho_{1-x}Gd_xNi_2$ and $HoNi_{2-y}Co_y$ alloys around hydrogen liquefaction temperature. Scripta Mater, 2020, 188: 302–306
60 Matsumoto KT, Hiraoka K. Magnetocaloric effect in Gd-based ferromagnet $GdZn_2$. J Magn Magn Mater, 2017, 423: 318–320
61 Oboz M, Talik E. Properties of the GdTX (T = Mn, Fe, Ni, Pd, X = Al, In) and $GdFe_6Al_6$ intermetallics. J Alloys Compd, 2011, 509: 5441–5446
62 Taskaev S, Khovaylo V, Skokov K, *et al.* Magnetocaloric effect in $GdNi_2$ for cryogenic gas liquefaction studied in magnetic fields up to 50 T. J Appl Phys, 2020, 127: 233906
63 Law JY, Franco V. Magnetocaloric composite materials. In: Brabazon D (ed.). Encyclopedia of Materials: Composites. Amsterdam: Elsevier, 2021, vol 2: 461–472
64 Law JY, Moreno-Ramírez LM, Blázquez JS, *et al.* Gd+GdZn biphasic magnetic composites synthesized in a single preparation step: Increasing refrigerant capacity without decreasing magnetic entropy change. J Alloys Compd, 2016, 675: 244–247
65 Gębara P, Díaz-García Á, Law JY, *et al.* Magnetocaloric response of binary Gd-Pd and ternary Gd-(Mn,Pd) alloys. J Magn Magn Mater, 2020, 500: 166175
66 Zhang Y, Yang Y, Xu X, *et al.* Excellent magnetocaloric properties in RE_2Cu_2Cd (RE = Dy and Tm) compounds and its composite materials. Sci Rep, 2016, 6: 34192
67 Romero-Muñiz C, Franco V, Conde A. Influence of magnetic interactions between phases on the magnetocaloric effect of composites. Appl Phys Lett, 2013, 102: 082402
68 Moreno-Ramírez LM, Law JY, Pramana SS, *et al.* Analysis of the magnetic field dependence of the isothermal entropy change of

inverse magnetocaloric materials. Results Phys, 2021, 22: 103933

Acknowledgements This work was supported by the National Natural Science Foundation of China (52071197), the Science and Technology Commission of Shanghai Municipality (19ZR1418300 and 19DZ2270200), AEI/FEDER-UE (PID2019-105720RB-I00), US/JUNTA/FEDER-UE (US-1260179), and Consejería de Economía, Conocimiento, Empresas y Universidad de la Junta de Andalucía (P18-RT-746). Guo D would like to acknowledge the support provided by China Scholarship Council (CSC) of the Ministry of Education, China (202006890050).

Funding note: Open Access funding provided thanks to the CRUE-CSIC agreement with Springer Nature.

Author contributions Zhang Y and Law JY designed the idea of the research. Guo D and Zhang Y performed the experiments. Guo D and Moreno-Ramírez LM performed the data analysis. Romero-Muñiz C contributed to the DFT calculations and analysis. Guo D, Moreno-Ramírez LM, and Law JY prepared the manuscript. All the authors contributed to the general discussion and review and editing. Franco V and Zhang Y contributed to the conceptualization and supervision.

Conflict of interest The authors declare that they have no conflict of interest.

Supplementary information Supporting data are available in the online version of the paper.

Dan Guo is a PhD student at the School of Materials Science and Engineering, Shanghai University (SHU), China. She is now a visiting scholar sponsored by the China Scholarship Council at the University of Seville, Spain. Her research interests focus on magnetic properties and magnetocaloric effect of heavy rare-earth-based compounds.

Jia-Yan Law obtained her PhD degree from the School of Materials Science and Engineering, Nanyang Technological University, Singapore, in 2012. Currently, she is a postdoctoral researcher at the University of Seville, Spain, leading the research line "Functional High-Entropy Alloys". In addition, her research interests include the development of magnetic and magnetocaloric materials, device and novel evaluation techniques as well as additive manufacturing.

Yikun Zhang is an associate professor at the School of Materials Science and Engineering, SHU (China) since 2016. She received her PhD degree in materials science from Northeastern University (China) in 2010. Her research focuses on designing and exploring low-temperature magnetic refrigeration materials.

RE_6Co_2Ga (RE = Ho, Dy or Gd) 低温磁制冷材料的一级相变和二级相变

郭丹[1,2], Luis M. Moreno-Ramírez[2], Carlos Romero-Muñiz[3,4], 张义坤[1*], Jia-Yan Law[2*], Victorino Franco[2], 王江[1], 任忠鸣[1]

摘要 具有正交Ho_6Co_2Ga型晶体结构的富稀土金属间化合物因其具备独特的磁性能而被关注，但它们的磁有序、磁相变类型以及磁热性能尚未见系统报道. 本文通过对RE_6Co_2Ga化合物中的稀土元素类型的调控，实现了材料相变类型从反铁磁(AF)到顺磁(PM)的变磁调控为铁磁(FM)到顺磁(PM)的转变. 此外，通过实验观察结合密度泛函理论(DFT)计算证明了Gd_6Co_2Ga的基态为铁磁态. 利用磁热效应的场依赖性关系结合Banerjee准则的判断标准研究表明，Ho_6Co_2Ga和 Dy_6Co_2Ga同时具备二级相变和一级相变特征，而在Gd_6Co_2Ga中只存在二级相变. 在0–5 T的磁场变化下，Ho_6Co_2Ga和Gd_6Co_2Ga的磁熵变分别在26和75 K附近达到最大值10.1和9.1 $J\,kg^{-1}\,K^{-1}$，而这两个温度分别接近于H_2液化和N_2液化温度. 优异的磁热性能使得RE_6Co_2Ga体系在低温磁制冷领域具有潜在的应用前景.

